Mass spectrometric study of discharges produced by a large-area dual-frequency–dual-antenna inductively coupled plasma source

2012 J. Phys. D: Appl. Phys. 45 475201

(http://iopscience.iop.org/0022-3727/45/47/475201)

J. Phys. D: Appl. Phys. **45** (2012) 475201 (8pp) doi:10.1088/0022-3727/45/47/475201

Mass spectrometric study of discharges produced by a large-area dual-frequency–dual-antenna inductively coupled plasma source

Anurag Mishra[1], Tae Hyung Kim[1], Kyong Nam Kim[1] and Geun Young Yeom[1,2]

[1] Department of Advanced Materials Science and Engineering, Sungkyunkwan University, Suwon, Gyeonggi-do 440-746, South Korea
[2] SKKU Advanced Institute of Nanotechnology (SAINT), Sungkyunkwan University, Suwon, Gyeunggi-do 440-746, South Korea

E-mail: gyyeom@skku.edu

Received 4 June 2012, in final form 17 September 2012
Published 30 October 2012
Online at stacks.iop.org/JPhysD/45/475201

Abstract
An energy-resolved quadrupole mass spectrometer is used to investigate the time-averaged ion energy distribution (IED) of positive ionic species in an Ar/CF_4 (90%/10%) discharge produced by dual-frequency–dual-antenna, next-generation large-area inductively coupled plasma source. The operating pressure is 10 mTorr. Two radio frequencies of 2 MHz (low frequency) and 13.56 MHz (high frequency) are used to initiate and sustain the discharge. The orifice of the mass spectrometer was 100 μm in diameter and placed at 30 mm below the ICP source and 20 mm outside the discharge volume.

It is observed that both of the frequencies have significant effect on IEDs of all prominent discharge species. The evolution of IEDs with power shows that the discharge undergoes a mode transition (E to H) as the applied power is increased. At a fixed value of $P_{13.56}$ MHz (250 and 500 W), the energy spread and the energy separation between two peaks of IEDs increase illustrating enhanced E-mode. Above $P_{13.56\,\mathrm{MHz}} = 500$ W, the IEDs show opposite trends, i.e. decreasing energy spread and energy separation between two peaks, showing the strengthening of H-mode. Increasing $P_{13.56}$ MHz at a fixed value of P_2 MHz has similar effects. A comparison of IEDs sampled at a fixed total power ($P_{13.56\,\mathrm{MHz}} + P_{2\,\mathrm{MHz}}$) demonstrates that an IED can be tailored by changing the power ratio ($P_{13.56}$ MHz/P_2 MHz).

(Some figures may appear in colour only in the online journal)

1. Introduction

Plasma processing is an indispensable tool in the microelectronics industry for manufacturing various electronic devices such as thin-film transistors, flat panel and liquid crystal displays [1–3]. The current trend in the microelectronics semiconductor industry, for fabrication of electronic devices, is to etch at a few tens of nanometre level. However, the device fabrication cost increases as the size of the electronic device reduces (as the etching resolution increases). One potential way to improve productivity and to optimize the fabrication cost of such microelectronic devices is to adopt processing on large-area wafers. For this reason, a significant research interest has evolved in developing large-area plasma sources for fabrication of next-generation microelectronics devices. According to a technology trend forecast, the wafer size will be 450 mm in diameter within a few years [4, 5] and the wafer size in the flat panel display industry is speculated to be 3000 × 3320 mm^2 (11th generation) in the near future. Device fabrication on large-area wafers poses a significant challenge to precisely

control the distribution of plasma species over the substrate. Over the last decade, many types of high-density and large-area plasma sources, based on different mechanisms of electromagnetic coupling to discharge and geometrical configurations, have been extensively investigated [6–20]. Due to the ability of being operated at low pressures (<10 mTorr) owing to strong power coupling through electromagnetic fields, high plasma density, easy plasma uniformity control and the separation between discharge production and ion acceleration mechanism, ICP sources have attracted significant research interest as potential large-area plasma sources. However, some problems (increased RF voltage drop across the antenna, decreased average power transfer efficiency to the discharge and increased azimuthal non-uniformity) are associated with the scaling up of conventional ICP sources. The azimuthal non-uniformity is particularly due to the standing wave effect. To avoid these problems associated with the scaling up of ICP sources, a novel approach of dual-frequency–dual-antenna (DFDA) inductively coupled plasma source has recently been proposed by our group [21]. From the ion flux measurements over the substrate region, it has been demonstrated that this approach (dual-frequency ICP source) is capable of producing a very high radially uniform ion flux over the substrate [21]. However, that study [21] is concentrated on investigating the discharge parameters. This study goes further and illustrates an investigation of ion energy distribution (IED) functions of various ionic species in the discharge produced by a DFDA-ICP source and demonstrates that by choosing a particular RF power ratio (P_2 MHz/$P_{13.56\,\mathrm{MHz}}$), the IED could be tailored for a specific application.

In the dry etching community, CF_4 has attracted much theoretical [22–25] and experimental [26–29] research interest for etching SiO_2 and plasma chamber cleaning processes [30–32]. Its relatively inert nature in its electronic ground state and the property of generating no stable excited states make it ideal for producing the desired neutral and ionic species in a controlled manner. Due to these properties and the wealth of data available about pathways for CF_4 kinetics [33–37], investigations of CF_4 plasmas serve as an important laboratory tool for extracting a better understanding of etching processes involving CF_x radicals and ions. This is the reason why we chose CF_4 as an investigation gas to understand the influence of power and frequency levels on IEDs. CF_3^+ is found as the major ionic species in the discharge [38]; however, other fluorocarbon ions (CF_2^+, CF^+) are also present in significant number. The main mechanism responsible for the production of fluorocarbons is the direct electron impact ionization of the parent molecule (CF_4), and it produces fluorocarbons in the order $CF_3^+ > CF_2^+ > CF^+$. The partial ionization cross-section measurements [38] show that the threshold energies for ionization of these species are 16 eV, 22 eV and 27 eV, respectively. The relatively lower ionization energy makes CF_3^+ the major ionic species produced by direct electron impact ionization. Another important mechanism responsible for discharge production is the direct electron impact ionization of dissociated fragments (CF_3, CF_2 and CF). The threshold energy necessary for dissociation of CF_4 is 12.5 eV [38] and there are a sufficient number of such electrons of 12.5 eV available in the discharge.

The IED function is an important, if not crucial, discharge parameter that determines the discharge etch properties such as etch chemistry, etch rate and etch profile of the substrate. Therefore, it is necessary, before using a new plasma source, to investigate how the IED depends on the operational parameters of the discharge produced by it. In the literature, many theoretical, numerical and experimental studies are found related to the investigation of IEDs [40–48]. Most of these studies were carried out in single- and dual-frequency CCP discharges and attempted to investigate the effect of low and high frequencies over ion flux distribution at the substrate and IEDs with the aim to realize independent control over ion flux and IEDs. Lee *et al* [43], using PIC/MCC simulation, numerically demonstrated that IED shape and spread can be controlled by the driving voltage in a single-frequency discharge and by the low-frequency voltage in a dual-frequency (2 MHz/27 MHz) CCP discharge. For IEDs in a single-frequency discharge, Kawamura *et al* published a review paper [49] detailing the theoretical and experimental aspects of IEDs, in the collisionless regime, arriving at the target in a radio-frequency discharge and illustrated that the ratio $\tau_{\mathrm{ion}}/\tau_{\mathrm{rf}}$ determines the nature of sheath, the sheath voltage waveform and the shape of IEDs. Benck *et al* [50] investigated the effect of pressure and gas ratio IED in an Ar/C_4F_6 inductively coupled discharge and demonstrated that the IEDs are significantly modified by time-varying sheath electric fields. Rao *et al* [38] studied the effect of pressure on IED shape in a single-frequency ICP discharge and demonstrated that the IEDs shift towards the low-energy end as the pressure increases at a constant RF power. However, there is no study found in the literature investigating IEDs in dual-frequency ICP discharges. This study addresses this issue with regard to a large-area DFDA inductively coupled plasma source. This experimental work investigates the influences of RF powers of low (2 MHz) and high frequencies (13.56 MHz) on IEDs of CF^+ and CF_3^+.

2. Experimental set-up

A detailed description of the plasma source can be found elsewhere [21]. The plasma source consists of two planar-spiral coils made of copper tube, 7 mm in diameter. The inner coil has 12 turns and a diameter of 320 mm, whereas the outer coil has 3 turns and outer diameter of 400 mm. RF powers at 2 MHz and 13.56 MHz are fed to the inner and outer coils via two separate matching networks, respectively.

A schematic of the experimental set-up and the acquisition instrumentations is shown in figure 1. The Ar/CF_4 discharge is operated in a cylindrical anodized aluminium chamber using an external type dual-antenna–dual-frequency ICP source, which is separated from the main processing chamber by a dielectric window. The chamber walls are electrically grounded and the gases in the chamber are evenly distributed using a multi-hole shower ring located along the periphery of the chamber. A base pressure of less than 3×10^{-6} mTorr is routinely achieved using a turbomolecular pump backed by a dry pump. The pressure inside the chamber is controlled using a mass flow controller (2900 series, Tylan) together with an adaptive pressure controller (PM-7, VAT) for the gate valve control.

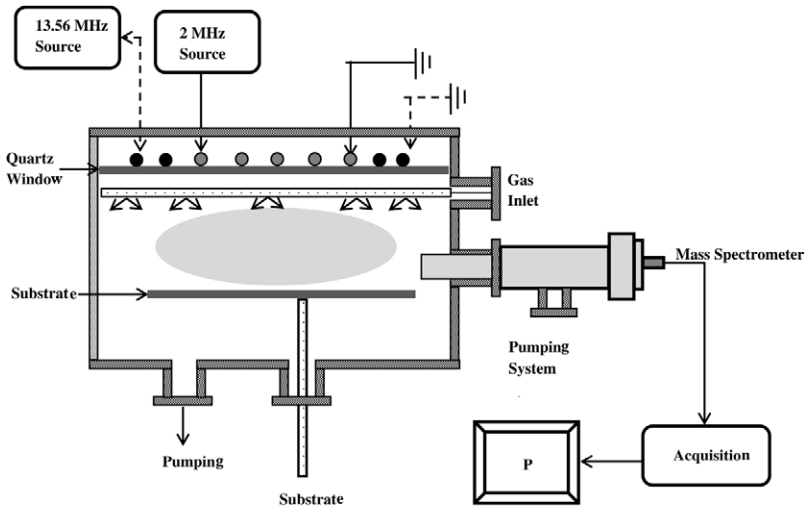

Figure 1. Schematic of the experimental set-up, electrical arrangement and acquisition system.

The inner and outer coils are energized by 2 MHz RF (NOVA-50 A, ENI) and 13.56 MHz RF (CX-5000S, COMDEL) power generators, respectively. The operating pressure is kept at 10 mTorr. P_2 MHz and $P_{13.56}$ MHz powers are varied from 250 W to 1000 W and from 0 W to 750 W, respectively.

An energy-resolved quadrupole mass spectrometer (PSM003, Hiden Analytical Ltd) is used to determine the IEDs. The ions are sampled into the mass spectrometer with a Bessel box energy filter at a pressure below 3×10^{-6} Torr achieved using a differential pumping system attached to the mass spectrometer. The mass spectrometer is operated in positive ion detection mode, which implements the scanning of energy at a fixed mass-to-charge ratio, i.e. the measurement of different ions' IEDs. To minimize the random error, every IED presented in this study is averaged over five individual scans.

The orifice of the mass spectrometer is 100 μm in diameter and is placed 30 mm below the ICP source and 20 mm outside the discharge volume. The IEDs are collected in time-average mode. The most dominant fluorocarbon ionic species is CF_3^+. However, other species such as Ar^+, CF^+, CF_2^+ and CF_4^+ are also detected in significant number. Additionally, ionic species SiF_x ($x = 0$–3) are also detected (not shown here) due to etching of the quartz window and subsequent reactions.

3. Results and discussion

To ensure the reproducibility and reliability of our measurements, a number of test measurements were carried out before performing the real experiments. When a variation in the plasma power or pressure occurs, the peak energy of the plasma changes. Therefore, the mass spectrometer was tuned in such a way that the instrument always operates under the optimum energy conditions in positive ion collection mode. It has been achieved by setting the 'Auto Tune' selected and 'SaveScanDev' deselected in the energy scan dialogue box in the scan tree.

In order to make a uniform criterion for comparison between IEDs of various ionic species sampled at different discharge parameters, they were normalized by dividing each number of counts (vertical axis) by their energy-integrated summation. Figure 3 shows the actual IEDs of CF_3^+ (31 amu) and its normalized IEDs, sampled under a particular condition. The IEDs for all experimental conditions were sampled at the energy resolution of 0.1 eV.

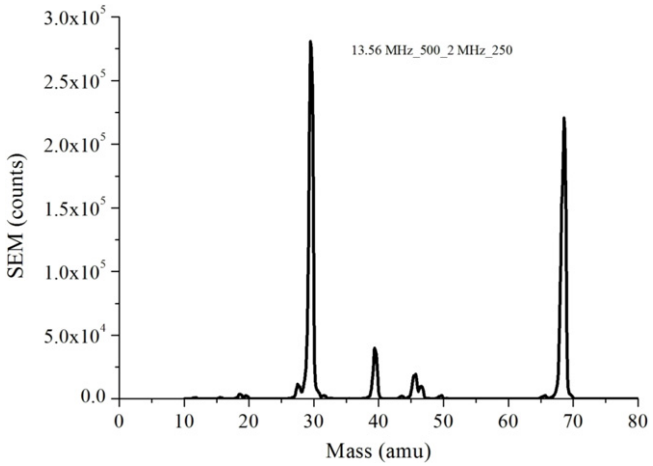

Figure 2. Plot of mass scan sampled by a mass spectrometer at a gas ratio of 90 : 10 (Ar : CF4). The high-frequency ($P_{13.56\,\mathrm{MHz}}$) and low-frequency ($P_{2\,\mathrm{MHz}}$) powers are kept at 250 W each.

The dominant ionic species were CF_3^+, CF_2^+, CF^+; however, under certain operational conditions (at high power levels), CF_4^+ and CF_4^{++} ions were also observed.

3.1. Effect of low-frequency power levels on IEDs

Figure 2 shows the mass-to-charge scan of the ions sampled in the quadrupole mass spectrometer when CF_4 concentration is 10% in the Ar/CF_4 gas mixture. From the figure, it can be seen that the dominant ionic species are CF_3^+ (69 amu) and CF^+ in the discharge. That is the reason these species are discussed in detail in this study. A peak observed at 28 amu is attributed to Si^+ sputtered from the quartz window located between the chamber and the antenna.

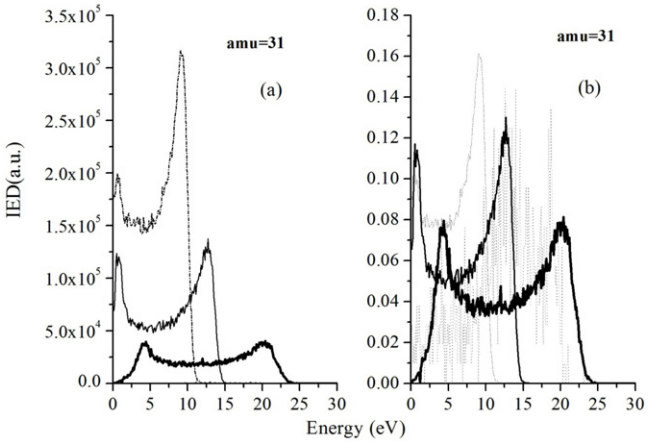

Figure 3. Plot of (*a*) actual and (*b*) normalized IED of CF^+ (31 amu) under a particular condition when $P_{13.56\,\mathrm{MHz}} = 00$ and $P_{2\,\mathrm{MHz}} = 250$ W.

Ar and CF_4 gas flow rates were 360 sccm and 40 sccm, respectively. The effect of low-frequency power levels on IEDs of CF^+(31 amu) is shown in figures 4(*a*)–(*c*). The low frequency was set at 2 MHz and the high frequency at 13.56 MHz. The measurements were carried out at three chosen power levels ($P_{13.56\,\mathrm{MHz}} = 000$, 250 and 750 W) of high frequency. The low-frequency power levels ($P_{2\,\mathrm{MHz}}$) were set at 250, 500, 750 and 1000 W. Figure 4(*a*) shows the IEDs at various low-frequency power levels, when the high-frequency power is kept zero. At $P_{2\,\mathrm{MHz}} = 250$ W, the discharge was lean (low plasma density) and therefore the number of ions collected by the PSM detector was very small, which, in turn, resulted in a very small number of counts produced by the PSM detector. Under this condition, noise dominated over the IED and therefore, peaks in the IED were not distinguishable. However, it can be seen that the IED spreads up to 20 eV. As P_2 MHz is increased up to at 500 W, the structure of the IED becomes clearer and broader, spreading up to 25 eV, with two distinct energy peaks, located at ∼4 eV and ∼20 eV, respectively. Comparing the IEDs collected at $P_{2\,\mathrm{MHz}} = 250$ and 500 W, two distinct features can be observed clearly, i.e. on transition from 250 to 500 W, the IED becomes broader by ∼5 eV (from 20 to 25 eV) and the separation of the two prominent energy peaks increases by 7.5 eV (from 8.5 to 16 eV). This observation is attributed to the strengthening of E-mode of operation and can be understood as follows.

In most of the etching plasmas operating at lower pressures, ion motion in the radio-frequency sheath is essentially collisionless as the sheath width is much smaller than the mean free path of ions. In the collisionless sheath, the shape of IED is determined by $\tau_{\mathrm{ion}}/\tau_{\mathrm{rf}} = \omega/\omega_{\mathrm{ion}}$, where $\tau_{\mathrm{ion}} = 2\pi/\omega$ is the time taken by the ion and $\tau_{\mathrm{rf}} = 2\pi/\omega_{\mathrm{rf}}$ is the rf period. For the low-frequency regime ($\tau_{\mathrm{ion}}/\tau_{\mathrm{rf}} \ll 1$), the ions cross the sheath in a small fraction of rf cycle and respond to the instantaneous sheath voltage. Therefore, their final energies depend on the phase at which the ions enter the sheath. This results in broad and bimodal IEDs. The separation between two energy peaks ΔE_{i} is the difference between the maximum

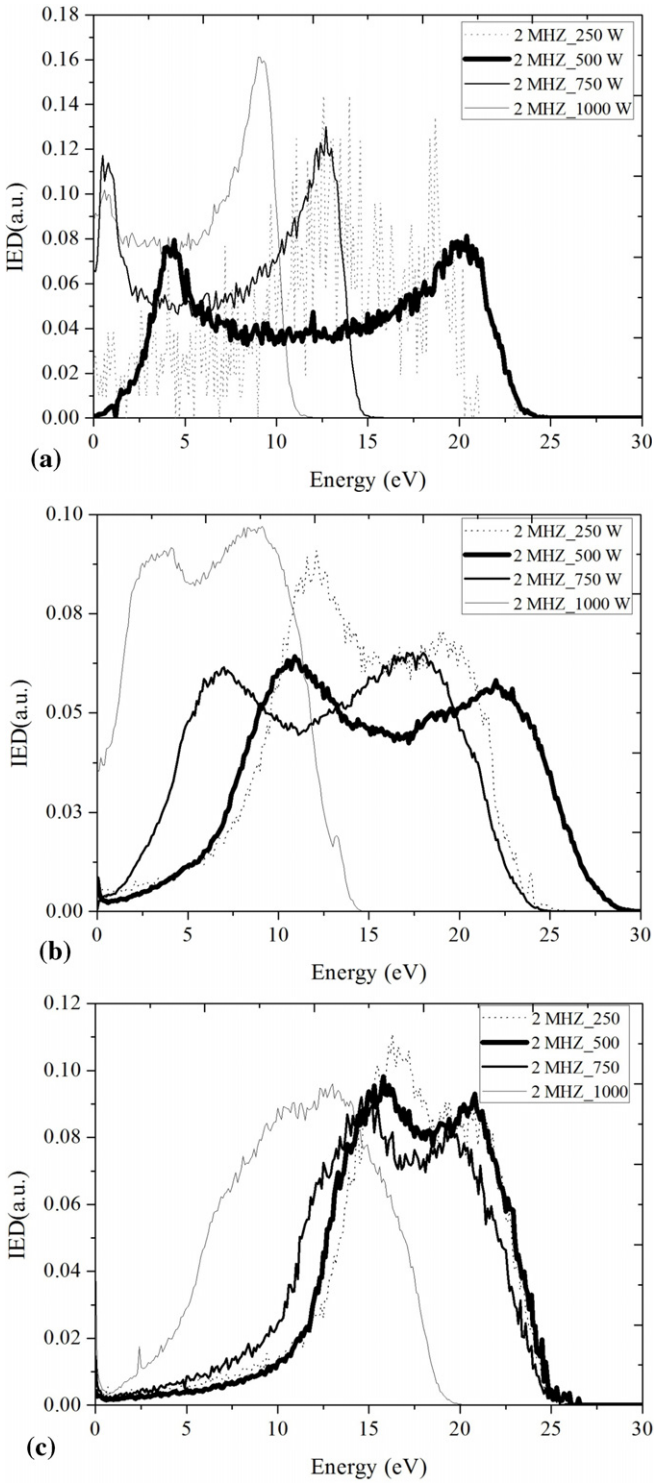

Figure 4. IEDs of CF^+ (31 amu) at (*a*) $P_{13.56\,\mathrm{MHz}} = 00$ W, (*b*) $P_{13.56\,\mathrm{MHz}} = 250$ W, (*c*) $P_{13.56\,\mathrm{MHz}} = 750$ W. Low-frequency power ($P_{2\,\mathrm{MHz}}$) is fixed at 250, 500, 750 and 1000 W. The operating pressure was 10 mTorr and gas ratio 90/10 (Ar/CF4).

and minimum voltage drop across the sheath and is directly proportional to $\tau_{\mathrm{rf}}/\tau_{\mathrm{ion}}$ [49]. The substitution of ion transit frequency in $\tau_{\mathrm{rf}}/\tau_{\mathrm{ion}}$ readily reveals that $\Delta E_{\mathrm{i}} \propto V_{\mathrm{s}}$ [49, 51], where V_{s} is the voltage drop across the sheath. Initially, when P_2 MHz increases (from 250 to 500 W), V_{s} increases and it results in increased ΔE_{i}, as observed in this study.

However, when $P_{2\,\mathrm{MHz}}$ exceeds above 500 W, the discharge operation transits from E- to H-mode (see figures 4(*a*) and 6(*a*)) and therefore, the power coupling mechanism to the discharge changes. In the H-mode of operation, the voltage drop across the sheath decreases and most of the power is dumped into the bulk plasma. This reducing voltage drop across the sheath (V_s) (in the region of $P_{2\,\mathrm{MHz}} > 500$ W) results in the lowering of the energy separation between the two energy peaks ΔE_i.

When P_2 MHz is increased from 500 to 750 W, the energy spread of the IED shrinks towards the lower energy side by ~9 eV (high-energy end, from ~24 to ~15 eV and separation between the two prominent energy peaks reduces by 4 eV (from ~16 to ~12 eV) (see figure 4(*a*)). The average voltage drop across the sheath, derived from the IED, $V_s = (E_1 + E_2)/2e$, where E_1 and E_2 are the energy of the two prominent peaks in the IED, decreases by ~2 V (from 8 to 6 V). It is also observed that the number of integrated counts in the IED increases significantly (not shown here), which indicates a sharp rise in the plasma density. These observed features (shrinking energy spread of the IED, decreasing ΔE_i, decreasing V_s and increasing plasma density) are the signature of discharge mode transition from a capacitively coupled to an inductively coupled one [52]. However, in a pure ICP discharge, the IED has a mono-modal structure [53] due to the predominant dc component in the plasma potential (V_p), owing to the collisionless sheath and no stray capacitance between the rf coils and the chamber walls. Therefore, it can be inferred that the IED at $P_{2\,\mathrm{MHz}} = 750$ W also has a capacitive component (bimodal structure).

When P_2 MHz is further increased up to 1000 W, the IED shifts more towards lower energy (~10 eV), the energy separation between the two peaks decreases to ~8 eV and V_s lowers to ~4 V (see figure 4(*a*)). It is also observed that the intensity of the first energy peak reduces significantly compared with second energy, i.e. the IED tends to be mono-modal. This suggests that the ICP component becomes more dominant than that of CCP under this operational condition [52].

Figures 4(*b*) and (*c*) show the IEDs sampled at $P_{2\,\mathrm{MHz}} =$ 250–1000 W, at two chosen high-frequency powers ($P_{13.56\,\mathrm{MHz}}$) of 250 W and 750 W, respectively. The salient features of figures 4(*b*) and (*c*) are similar to figure 4(*a*). However, from the comparison of figures 4(*a*)–(*c*), it can be clearly seen that the value of ΔE_i decreases with increasing $P_{13.56}$ MHz, tending towards the mono-modal IED (at $P_{13.56\,\mathrm{MHz}} = 750$, $P_{2\,\mathrm{MHz}} =$ 1000 W, figure 4(*c*)). The IEDs shift towards the higher energy side and the spread of IEDs (FWHM) decreases as $P_{13.56\,\mathrm{MHz}}$ increases from 0 to 750 W. The rf power dependence of ΔE_i, V_s and FWHM is shown in figures 5(*a*)–(*c*). It can be seen from figures 5(*a*)–(*c*) that the values of ΔE_i, V_s and FWHM initially increase with RF power from $P_{2\,\mathrm{MHz}} =$ 250–500 W, after that decrease with RF power from $P_{2\,\mathrm{MHz}} =$ 500–1000 W. The decreasing values of ΔE_i, V_s and FWHM with $P_{2\,\mathrm{MHz}}$ (500–1000 W) are an indication of the strengthening of H-mode (inductive) in the discharge. The increasing trend of ΔE_i,V_s and FWHM with $P_{2\,\mathrm{MHz}} =$ 250–500 W is due to the discharge being in E-mode (capacitive).

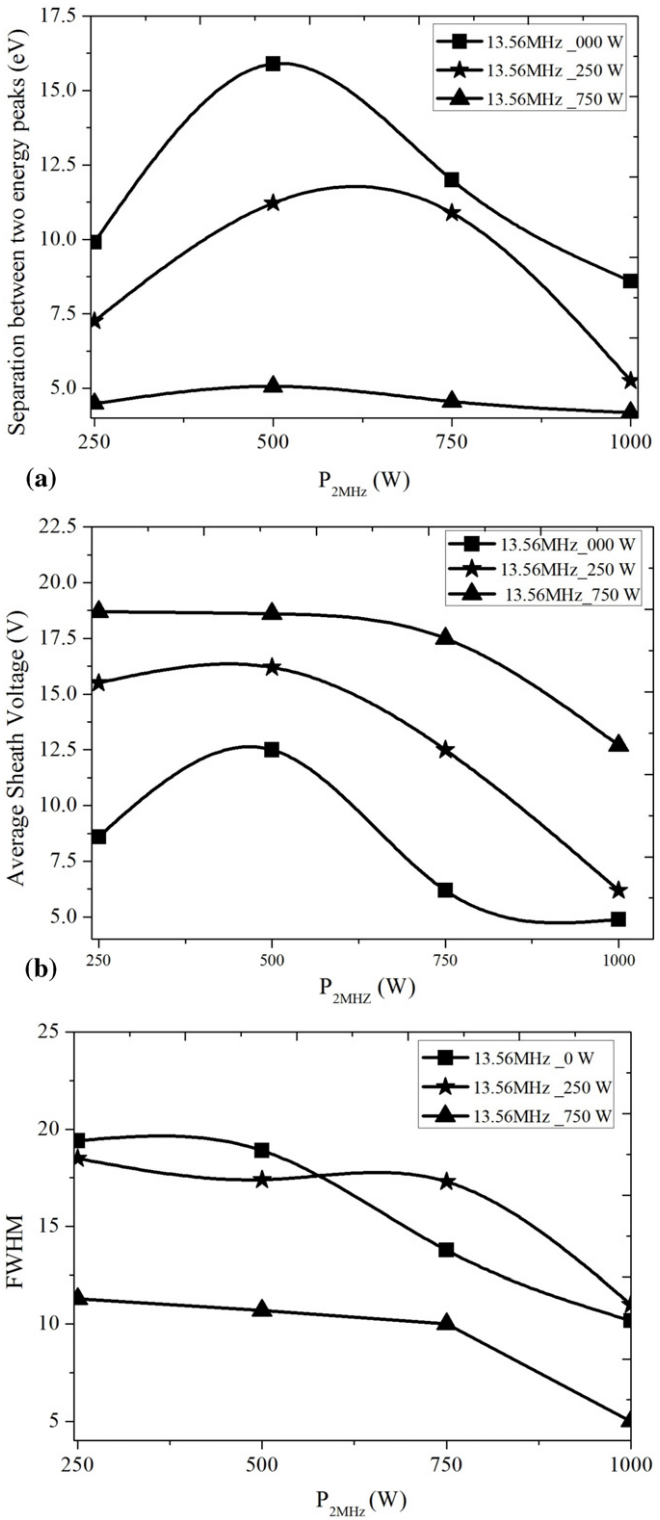

Figure 5. Plot of (*a*) energy separation between two energy peaks in IEDs, (*b*) average sheath voltage, (*c*) FWHM of IEDs versus low-frequency power. All these parameters are derived from IEDs. The IEDs are sampled at three chosen high-frequency powers of 000, 250 and 750 W.

Similar trends in IEDs are found for other ionic species, such as CF_2^+ (50 amu), CF_3^+ (69 amu), CF_4^+ (88 amu) and CF_4^{++} (44 amu), with increasing $P_{2\,\mathrm{MHz}}$. The trends in IEDs for CF_3^+ (69 amu) are shown in figures 6(*a*)–(*c*).

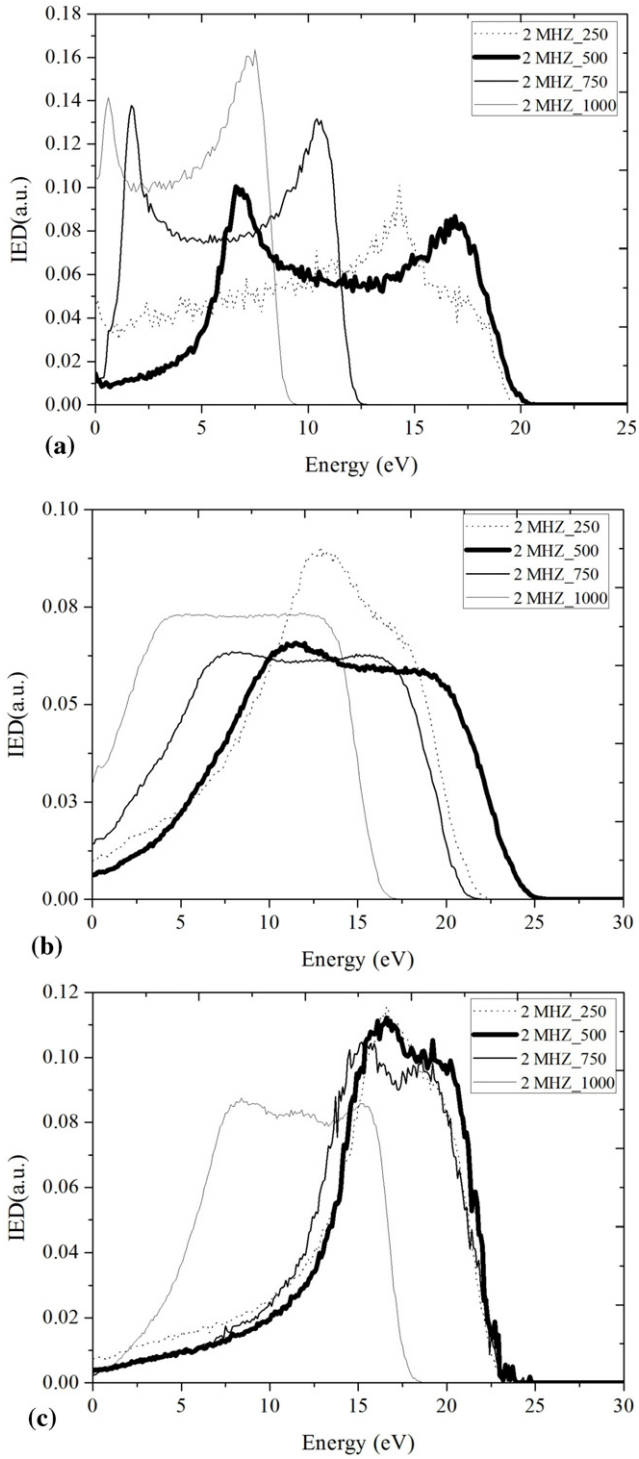

Figure 6. IEDs of CF_3^+ (69 amu) at (*a*) $P_{13.56\,\mathrm{MHz}} = 00$ W, (*b*) $P_{13.56\,\mathrm{MHz}} = 250$ W, (*c*) $P_{13.56\,\mathrm{MHz}} = 750$ W. Low-frequency power ($P_{2\,\mathrm{MHz}}$) was varied as 250, 500, 750 and 1000 W. The operating pressure was 10 mTorr and gas ratio 90/10 (Ar/CF4).

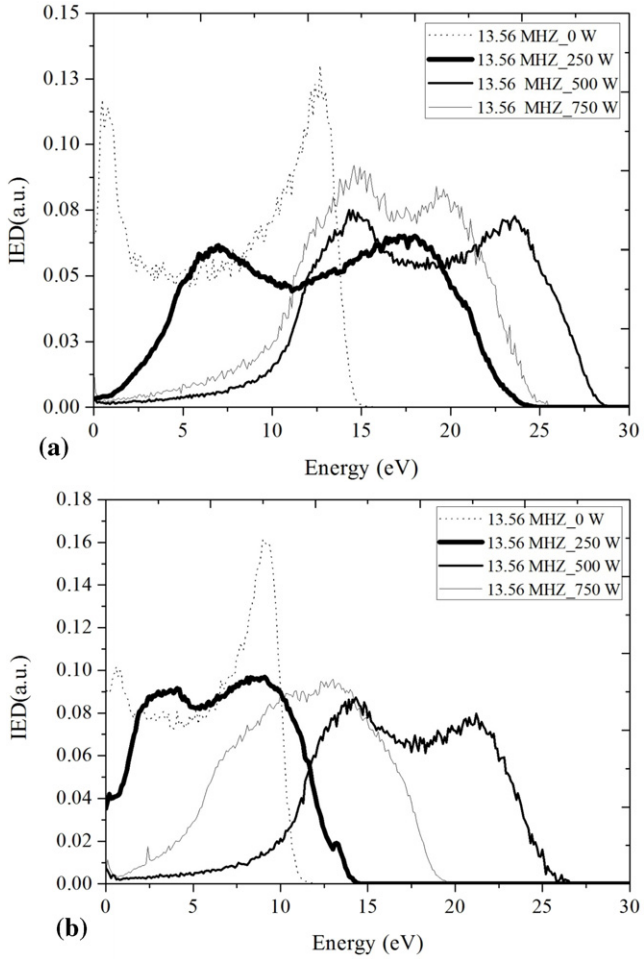

Figure 7. IEDs of CF^+ (31 amu) at (*a*) $P_{2\,\mathrm{MHz}} = 750$ W, (*b*) $P_{2\,\mathrm{MHz}} = 1000$ W. High-frequency power ($P_{13.56\,\mathrm{MHz}}$) was varied as 000, 250, 500 and 750 W. The operating pressure was 10 mTorr and gas ratio 90/10 (Ar/CF4).

3.2. Effect of high-frequency power levels on IEDs

The effect of high-frequency power levels ($P_{13.56}$ MHz) on the IEDs at fixed $P_{2\,\mathrm{MHz}}$ of 750 and 1000 W is shown in figures 7(*a*) and (*b*) for CF^+ (31 amu). $P_{13.56\,\mathrm{MHz}}$ is varied from 0 to 750 W in steps of 250 W. As can be seen from figures 7(*a*) and (*b*), the IEDs have similar trends (strengthening of E-mode, transition from E- to H-mode and then strengthening of H-mode) as low-frequency effects on IEDs shown in figures 4(*a*)–(*c*). The trends in ΔE_i, V_s and FWHM are also similar with high-frequency power levels. Comparing figures 7(*a*) and (*b*) readily reveals that as $P_{2\,\mathrm{MHz}}$ increases from 750 to 1000 W, the energy spread of IEDs reduces from ∼30 to 25 eV (at $P_{13.56\,\mathrm{MHz}}$) indicating the strengthening of H-mode in the discharge.

To investigate the effect of low- and high-frequency power levels individually on the IED, a graph (see figure 8) is plotted with increasing $P_{13.56}$ MHz. The total power was kept fixed at 1000 W. $P_{13.56\,\mathrm{MHz}}$ is increased from 250 to 750 W. Therefore, P_2 MHz decreases from 750 to 250 W. As the high-frequency power increases, at a fixed total power of 1000 W, FWHM and the separation between two energy peaks in IEDs decrease, tending from bimodal to mono-modal IED and therefore, indicating the increasing H-mode character in the discharge. The IED shifts towards the higher energy end (0.2 eV–7.2 eV) as the high-frequency power increases. Therefore, it can be inferred that high-frequency power content not only strengthens the H-mode but also enhances the energy of ionic species, and it can be concluded that a specific combination of power ratios ($P_{13.56}$ MHz/$P_{2\,\mathrm{MHz}}$) can tailor the IED specific

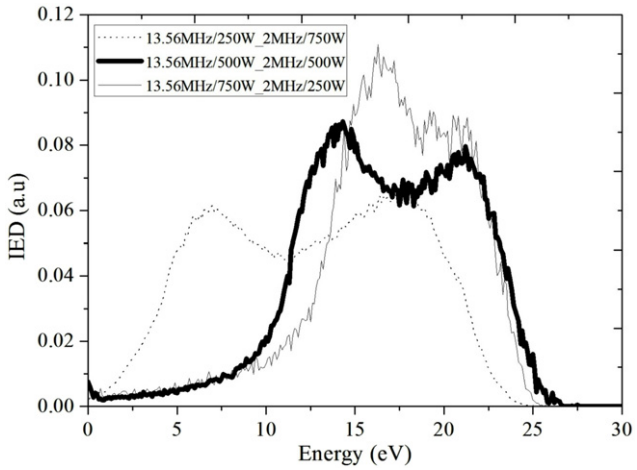

Figure 8. Plot of IEDs of CF^+ at a fixed total power of 1000 W. $P_{13.56}$ MHz was increased from 250 to 750 W. Therefore, P_2 MHz was reduced from 750 to 250 W to keep the total power fixed at 1000 W. The operating pressure was 10 mTorr and gas ratio 90/10 (Ar/CF4).

for a particular application. This tailoring of IEDs by varying the power ratio ($P_{13.56\,\mathrm{MHz}}/P_{2\,\mathrm{MHz}}$) could be attributed to the frequency coupling effect. The sheath resistance and ion-dissipated power in the sheath decrease with the driving frequency; the power dissipation mode transition takes place from the ion-dominated power dissipation to the electron-dominated power dissipation as the frequency increases [54]. As the mode transition (E–H) depends on the excitation frequency, at a particular power level ($P_{13.56\,\mathrm{MHz}} = P_2$ MHz), the low excitation frequency (2 MHz) might be operating in E-mode and the high excitation frequency (13.56 MHz) in H-mode. In E-mode, the sheath dynamics plays an important role and therefore could control the shape of IEDs, whereas sheath effects are no more effective in H-mode and this causes higher ionization. Therefore, by choosing a suitable ratio of RF power levels ($P_{13.56}$ MHz/P_2 MHz), the IEDs can be tailored as observed in this study.

4. Conclusions

Time-averaged ion energy distributions (IEDs) of positive ionic species in a discharge of Ar/CF_4 (90%/10%) produced by a dual-frequency–dual-antenna (DFDA), next-generation large-area inductively coupled plasma source are investigated using an energy-resolved quadrupole mass spectrometer (PSM003).

The effect of both excitation frequencies is observed on IEDs of all prominent discharge species. At a fixed RF power at high frequency (13.56 MHz), the IEDs shrink towards the lower energy side with the increase in RF power at low frequency (2 MHz) and the energy separation between two prominent peaks in IEDs decreases. The effect of increasing of RF power at high frequency (13.56 MHz), at a fixed RF power of low frequency, is to extend IEDs towards the higher energy side; however, the energy separation between two prominent energy peaks decreases in this case as well.

This experimental study demonstrates that dual-frequency ICPs could be used as an effective tool to tailor IEDs, with regard to a specific application by choosing a proper power ratio ($P_{13.56}$ MHz/$P_{2\,\mathrm{MHz}}$) at a fixed total power and therefore could control the discharge chemistry to better tailor the etch/deposition profile of the wafer.

Acknowledgments

This work was supported by the Global Leading Technology Program of the Office of Strategic R&D Planning (OSP) funded by the Ministry of Knowledge Economy, Republic of Korea. This work was also supported by the Industrial Technology Development Program (10039212, Core Technology Development for Next Generation LCD Equipment) funded by the Ministry of Knowledge Economy (MKE, Korea).

References

[1] Chang C Y and Sze S M 1996 *ULSI Technology* (New York: McGraw-Hill) p 329
[2] Hopwood J 1992 *Plasma Sources Sci. Technol.* **1** 109
[3] Kahoh M, Suzuki K, Tonotani J, Aoki K and Yamage M 2001 *Japan. J. Appl. Phys.* **40** 5419
[4] International Technology Roadmap for Semiconductor, 2009 edition http://www.itrs.net
[5] Collision W Z, Ni T O and Barnes M S 1998 *J. Vac. Sci. Technol.* A **16** 100
[6] Yang Y and Kushner M J 2010 *J. Appl. Phys.* **108** 113306
[7] Hong S P, Lim J H, Gweon G H and Yeom G Y 2010 *Japan. J. Appl. Phys.* **49** 080217
[8] Kim K N, Lim J H, Yeom G Y, Lee S H and Lee J K 2006 *Appl. Phys. Lett.* **89** 251501
[9] Gweon G H, Lim J H, Kim K N, Hong S P, Min T H and Yeom G Y 2010 *Vacuum* **84** 823
[10] Lim J H, Kim K N, Gweon G H, Park J B and Yeom G Y 2009 *Plasma Chem. Plasma Process.* **29** 251
[11] Kim K N, Lim J H and Yeom G Y 2009 *Japan. J. Appl. Phys.* **48** 116006
[12] Kim K N, Lim J H, Lim W S and Yeom G Y 2010 *IEEE Trans. Plasma Sci.* **38** 2 133
[13] Lim J H, Kim K N, Park J K, Lim J T and Yeom G Y 2008 *Appl. Phys. Lett.* **92** 051504
[14] Setsuhara Y, Takenaka K, Ebe A and Nishisaka K 2007 *Plasma Process. Polym.* **4** S628
[15] Lim J H, Kim K N and Yeom G Y 2007 *Plasma Process and Polymers* **4** S999
[16] Chen F F and Chang J P 2002 *Lecture notes on Principles of Plasma Processing* (New York: Kluwer/Plenum)
[17] Lieberman M A, Booth J P, Chabert P, Rax J M and Turner M M 2002 *Plasma Sources Sci. Technol.* **11** 283
[18] Chabert P 2007 *J. Phys. D: Appl. Phys* **40** R63
[19] Volynets V, Shin H, Kang D and Sung D 2010 *J. Phys. D: Appl. Phys.* **43** 085203
[20] Bera K 1366 *IEEE Trans. Plasma Sci.* **36** 4
[21] Mishra A, Kim K N, Kim T H and Yeom G Y 2012 *Plasma Sources Sci. Technol.* **21** 035018
[22] Kamimura K, Iyanagi K, Nakano N and Makabe T 1999 *Japan. J. Appl. Phys.* **38** 4429
[23] Kondo K, Kuroda H and Makabe T 1994 *Appl. Phys. Lett.* **65** 31
[24] Rauf S and Kushner M 1997 *Appl. Phys.* 82 2805
[25] Zhang D and Kushner M J 2000 *J. Vac. Sci. Technol.* A **18** 2661
[26] Hancock G, Sucksmith J P and Toogood M T 1990 *J. Phys. Chem.* **94** 3269

[27] Booth J, Cunge G and Neully F 1998 *Plasma Sources Sci. Technol.* **7** 423–30
[28] Wanm Z, Liu J and Lamb H H 1995 *J. Vac. Sci. Technol.* A **13** 2035
[29] Booth J P, Hancock G, Perr N D and Toogood M J 1989 *J. Appl. Phys.* **66** 5251
[30] Chow T P and Stecki A 1984 *J. Electrochem. Soc.* **131** 2325
[31] Wan Z, Liu L and Lamb H H 1995 *J. Vac. Sci. Technol.* A **13** 2035
[32] Zhang Y, Oehrlein G S and Bell F H 1996 *J. Vac. Sci. Technol.* A **14** 2127
[33] Hikosaka Y, Nakamura N and Sugai H 1994 *Japan. J. Appl. Phys.* **33** 2157
[34] Pender J T P and Brake M L 1998 *IEEE Trans. Plasma Sci.* **26** 1583
[35] Rauf S and Kushner M J 1997 *J. Appl. Phys.* **82** 2805
[36] Christophorou L G, Olthoff J K and Rao M V V S 1996 *J. Phys. Chem. Ref. Data* **25** 1341
[37] Peko B L, Dyakov I V, Champion R L, Rao M V V S and Olthoff J K 1999 *Phy. Rev.* E **60** 7447
[38] Rao M V V S, Sharma S P and Meyyappan M 2002 *Plasma Sources Sci. Technol.* **11** 397–406
[39] Fisher E R, Weber M E and Armentrout P B 1990 *J. Chem. Phys.* **92** 2296
[40] Boyle P C, Ellingboe A R and Turner M M 2004 *J. Phys. D: Appl. Phys.* **37** 697
[41] Kim H C, Lee J K and Shon J W 2003 *Phys. Plasmas* **10** 4545
[42] Georgieva V and Bogaerts A 2005 *J. Appl. Phys.* **98** 023308
[43] Lee K, Manuilenko O V, Babaeva N Y, Kim H C and Shon J W 2005 *Plasma Sources Sci. Technol.* **14** 89
[44] Georgieva V, Bogaerts A and Gijbels R 2003 *J. Appl. Phys.* **94** 3748
[45] Georgieva V, Bogaerts A and Gijbels R 2004 *Phys. Rev.* E **69** 026406
[46] Wang S, Xu X and Wang Y N 2007 *Phys. Plasmas* **14** 113501
[47] Guan Z Q, Dai Z L and Wang Y N 2005 *Phys. Plasmas* **12** 123502
[48] Wu A, Lieberman M A and Verboncoeur J V 2007 *J. Appl. Phys.* **101** 056105
[49] Kawamura E, Vahedi V, Lieberman M A and Birdsall C K 1999 *Plasma Sources Sci. Technol.* **8** R45–64
[50] Benck E C, Goyette A and Wang Y 2003 *J. Appl. Phys.* **94** 3 1382
[51] Chabert P and Braithwaite N 2011 *Physics of Rado-Frequency Plasmas* (Cambridge: Cambridge University Press)
[52] Kang D H, Lee D K, Kim K B, Lee J J and Joo J 2004 *Appl. Phys. Lett.* **84** 17 3283
[53] Woodworth J R, Riley M E, Meister D C, Aragon B P, Le M S and Swan H H 1996 *J. Appl. Phys.* **80** 1304
[54] You S J, Kim H C, Chung C W, Chang H Y and Lee J K 2003 *J. Appl. Phys.* **94** 12 7422